PAPER

Enhanced antibacterial efficacy: rapid analysis of silver-decorated azithromycin-infused Soluplus® nanoparticles against *E. coli* and *S. epidermidis* biofilms

Murali Mohan Jaligam, [ID] [a] Chisato Takahashi, [ID] *[b] Benjamin Heidt [ID] [a] and Amy Q. Shen [ID] *[a]

The escalating threat of antibiotic-resistant bacterial biofilms necessitates innovative antimicrobial strategies. This study introduces silver-decorated azithromycin-infused Soluplus® nanoparticles (Ag-AZI-Sol NPs) synthesized *via* a controlled emulsion diffusion method to ensure sustained release of antimicrobial silver ions for over six hours—a critical factor for continuous antibacterial efficacy. The efficacy of these nanoparticles was evaluated against biofilms formed by *Escherichia coli* (*E. coli*) and *Staphylococcus epidermidis* (*S. epidermidis*), pathogens that cause hospital-acquired infections. Concentrations of 5 and 10 μg mL^{-1} of Ag-AZI-Sol NPs induced significant morphological changes within the biofilms, disrupting the bacterial extracellular matrix as observed using scanning electron microscopy (SEM). This disruption peaked between two and six hours, coinciding with damage to bacterial cells by the silver ions. Antibacterial assay measurements confirmed a significant reduction in the growth rate among the Ag-AZI-Sol NP-treated bacteria compared with controls. Electrochemical analysis using laser-induced graphene (LIG) and chronoamperometry revealed a decline in current, indicating an effective antibacterial effect. This innovative biosensing technique makes use of the high conductivity and surface area of LIG to detect changes in bacterial activity quickly and sensitively. Our findings highlight the potent microbicidal properties of Ag-AZI-Sol NPs and suggest diverse applications from food processing to medical device coatings.

1. Introduction

Bacterial biofilms, complex structures consisting of bacterial aggregates embedded in an extracellular matrix of proteins and polysaccharides, pose major challenges in the realms of medicine and biomedical engineering.[1,2] These biofilms offer pathogens a multitude of advantages, shielding them from physical stresses like shear forces, pH changes, antiseptics, and antibiotics, while allowing them to evade immune detection, thus fostering an ideal environment for bacterial proliferation.[3] Eradicating bacterial biofilms is particularly difficult, and this poses significant concerns for medical implants, such as catheters and orthopedic implants,[4,5] which are prone to

biofilm formation due to their material properties such as surface charge, surface energy and hydrophobicity.[6]

While antibiotics often struggle to reach their full potential, antibacterial nanoparticles, especially silver nanoparticles (Ag NPs), have shown great promise in combating biofilms.[7,8] Ag NPs typically range in size from 1 to 100 nm[9,10] with a large surface to volume ratio that endows them with versatile properties. Beyond their efficacy against antibiotic-resistant biofilms, Ag NPs have found applications in diverse fields including optics,[11] medical diagnostics,[12,13] catalysis,[14] anti-cancer therapeutics,[15] and food packaging[16] for enhanced food safety.[17,18]

Silver nanoparticles can be synthesized using either bottom-up or top-down approaches. In the bottom-up method, single metal ions are assembled into larger nanoparticles, while the top-down method involves reducing larger metal pieces until they reach nano size.[19] The fabrication methods can be categorized into physical, chemical, and biological methods. Common physical methods include laser ablation and evaporation–condensation approaches.[10,19] Chemical methods, the most common approach, involve the reduction

[a]Micro/Bio/Nanofluidics Unit, Okinawa Institute of Science and Technology Graduate University, 1919-1 Tancha, Onna-son, Kunigami-gun, Okinawa, 904-0495, Japan. E-mail: amy.shen@oist.jp
[b]National Institute of Advanced Industrial Science and Technology (AIST), 205 Sakurazaka 4-chome, Moriyama-ku, Nagoya, Aichi, 463-8560, Japan. E-mail: nagoya.u.takahashi@gmail.com

and subsequent aggregation of metal salts, exemplified by techniques like the Brust–Schiffrin method.[10,19] Biological methods utilize living cells and their natural reducing agents to create nanoparticles, avoiding many hazardous components of physical and chemical fabrication.[10,19] Despite their intriguing properties, Ag NPs can be unstable and prone to oxidation and aggregation, particularly under physiological conditions.[20,21] Therefore, they must be stabilized, which can be achieved using surfactants, small ligands, or bigger molecules such as polymers.[9,22] Common stabilizers for Ag NPs include polyethylene glycol, polyvinyl alcohol, polymethylmethacrylate, and biologically derived polymers and proteins such as chitosan and bovine serum albumin.[9,10]

A new type of polymer, polyvinyl caprolactam polyvinyl acetate polyethylene glycol – a graft copolymer, known as Soluplus (Sol), has been developed to enhance the solubility of challenging medications. Our previous work demonstrated the efficacy of Sol as a stabilizer and carrier for Ag NPs.[23,24] Building on this, our current research investigates the effects of Ag NPs and azithromycin (AZI) conjugated with Soluplus on *E. coli* and *S. epidermidis* using scanning electron microscopy, optical density measurement, and electrochemical studies using laser-induced graphene (LIG) electrodes. LIG electrodes were fabricated by using a laser to transform an organic surface into a layer of highly electrically conductive graphene.[25] Specifically, we evaluated the efficacy of Ag-AZI-Sol NPs against biofilms of *E. coli* and *S. epidermidis*, observing significant disruption with SEM, particularly at between two and six hours. Electrochemical analysis using LIG revealed consistent antibacterial action. OD measurements and assay measurements demonstrated reduced bacterial growth. These findings highlight the potent antimicrobial properties of Ag-AZI-Sol NPs and offer valuable insights into strategies for combating biofilm formation.

2. Experimental methods

2.1 Materials and instrumentation

A polyimide sheet (HJA-A4-225 μm) with an A4 size of 210 × 297 mm and a thickness of 225 μm was procured from Hokushin, Japan. LB broth powder and agar were purchased from Sigma-Aldrich. *E. coli* (ATCC 8739) and *S. epidermidis* (ATCC 14990) were purchased from ATCC (American Type Culture Collection). Mill-Q water (18.2 MΩ cm) was used throughout all the experiments. The silver-decorated AZI-incorporated Sol nanoparticles (Ag-AZI-Sol NPs) were made using $AgNO_3$ and $NaBH_4$, which were acquired from Kishida Chemical Co. and Nacalai Tesque Inc., Japan. A BacLight bacterial viability kit was procured from Life Technologies Co., Japan (catalog number L-13152). The hydrophilic ionic liquid (1-butyl-3-methylimidazolium tetrafluoroborate [BMIM][BF_4]) for the preparation of the SEM sample was purchased from Kanto Chemical Co., Japan.

An Epilog CO_2 laser (Fusion Pro-48) with a maximum power of 120 W and a laser engraving speed of 4.2 m s^{-1} was pro-

cured from Epilog Lasers, USA. A laser microscope (Keyence VK-X100 series) was purchased from Keyence Corporation, USA. A four-point probe was purchased from Ossila Ltd, UK. A portable potentiostat (Sensit BT) was procured from Palmsens BV, the Netherlands. An incubator shaker (Innova 42) was purchased from Eppendorf. A UV spectrophotometer (UV-1800) was purchased from Shimadzu Corporation. Scanning electron microscopy (SEM) analysis was performed using a JSM 7900F and field emission SEM (FE-SEM) was performed using a JXA-8530FA from JEOL Co., Japan. A Zetasizer Nano (ZS90) was procured from Malvern Instruments Ltd, Malvern, UK.

2.2 Bacteria culture protocol

The guidelines of the ATCC (American Type Culture Collection) were followed in cultivating the bacteria. Luria–Bertani (LB) medium was prepared in 200 ml of DI water by mixing 4 g of agar and 3.6 g of LB broth. After plating the bacterial strains (*E. coli* and *S. epidermidis*) onto an agar plate, they were kept at 37 °C overnight to grow. Single cultures were then added to aliquots of LB broth and allowed to grow overnight at 37 °C on a shaker.

2.3 Ag-AZI-Sol particle synthesis

The synthesized Ag-AZI-Sol NPs contain "Sol", an amphiphilic material capable of trapping drug molecules. The Ag-AZI-Sol NPs are silver-decorated azithromycin-incorporated (AZI) nanoparticles synthesized using Soluplus® as a carrier material. These nanoparticles have a core–shell structure with azithromycin encapsulated within a polymeric matrix, while silver ions are intercalated on the surface to prevent agglomeration, as shown in Fig. 1a.

The Ag-AZI-Sol NPs were prepared using the emulsion solvent diffusion method.[23] Initially, Sol NPs at 70 mg were dispersed in purified water (100 mL), followed by the addition of $AgNO_3$ solution (1 mg mL^{-1}, 1 mL). The mixture was subjected to vortex stirring for an additional 30 min at 150 rpm. $NaBH_4$ (30 mg) was then added, mixed for 1 min, and stirred for 2 h at 1000 rpm. Subsequently, the mixture was dialyzed using a semipermeable membrane. The resulting dispersion was freeze-dried.
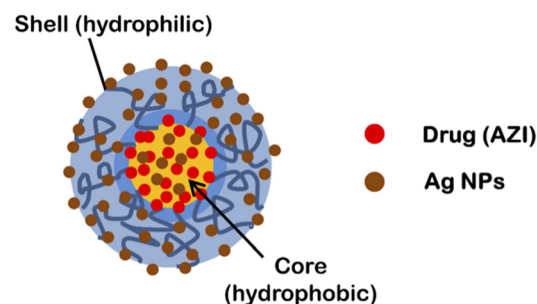

Fig. 1 Schematic representation of Ag-AZI-Sol NPs.

2.4 Quantification of silver ion release

Atomic absorption spectroscopy was employed to quantify Ag ion release for a given time duration. Previous investigations examined Ag ion release up to 120 minutes, while our study extends the analysis to 360 minutes. Fig. 2 illustrates the kinetics of the released silver ions over time, depicting rapid release within the initial 5 minutes, gradually increasing over time. Approximately 5% of the Ag ions were released within the first 5 minutes, followed by a gradual rise to 35% at the 360-minute mark. This prolonged release suggests the potential of Ag-AZI-Sol NPs for sustained antibacterial activity.

The particle size and zeta potential of the plain Sol and Ag-AZI-Sol NPs were determined and are tabulated in Table 1.

2.5 Fabrication of LIG electrodes

Recent studies have revealed the remarkable antibacterial properties of graphene and its composite materials, exhibiting increased toxicity against various bacteria, including Gram-positive and Gram-negative bacteria.[26,27] Traditional graphene synthesis methods are tedious and complicated to develop. Recent advancements have shown that graphene layers can be efficiently produced on polyimide sheets using CO_2 and blue lasers, a technique known as Laser-Induced Graphene (LIG).[28] LIG offers superior properties such as high conductivity, large surface area, and intrinsic charge carrier characteristics, making it highly suitable for diverse sensor applications.[29] As the name implies, LIG employs a laser to convert an organic surface into a highly conductive graphene layer. While polyimide is a typical substrate, LIG has shown versatility by working on various organic materials, from cloth to food products like potatoes and coconuts.[26–30] Its exceptional attributes and straightforward fabrication process render LIG particularly appealing for biosensing applications.
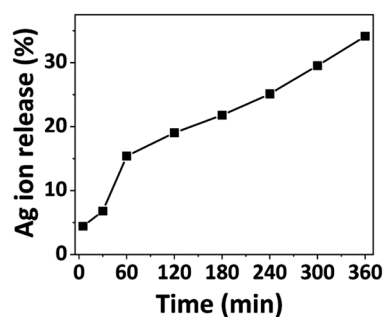
In this work, we developed a straightforward, affordable, and compact miniaturized LIG electrochemical platform for antibacterial studies. Using CorelDRAW software, electrodes were designed with dimensions of 20 mm × 1 mm (length × width). The electrode design was saved in portable document format (.pdf) and transferred to a CO_2 laser. We varied the power and speed of the laser according to different combinations, as detailed in Table 2, to create highly conductive electrodes. The maximum power (120 W) and laser speed (4.2 m s^{-1}) of the CO_2 laser were set at 100%. The percentage setting allows users to adjust the power and speed of the laser according to the specific requirements of their engraving task.

The resulting LIG electrodes exhibited a porous nature and non-uniform thickness. The average thickness of the LIG was determined using a laser microscope and is presented in Table 2. Subsequently, the conductivity of the LIG was measured using an Ossila four-point probe and the corresponding values are listed in Table 2. The data shown in Table 2 revealed that LIG formation did not occur at lower power levels (2.5%) with speeds of 10%, 7.5%, and 5%. However, the conductivity values gradually increased for a power level of 10% with speeds of 10%, 7.5%, 5%, and 2.5%, indicating that higher power and lower speeds were optimal for developing highly conductive electrodes. Notably, the highest conductivity of 1430 S m^{-1} was achieved with a power level of 10% and a speed of 2.5%.

The optimal parameters (power 10% and speed 2.5%) of the CO_2 laser were used to fabricate a three-electrode system, resulting in morphological structures, as depicted in Fig. 3. Prior to laser engraving, polyimide sheets were precleaned with isopropanol. The miniaturized electrochemical platform was assembled following the sequential steps, as illustrated in Fig. 4a–c. An overview of the complete setup is shown in Fig. 4d. In the electrode configuration, one electrode was modified with Ag/AgCl ink to serve as the reference electrode, while the remaining two bare LIG electrodes functioned as counter and working electrodes. A consistent sample volume

Fig. 2 Percentage of silver ion release from the Ag-AZI-Sol particles at various time intervals (in minutes).

Table 1 Particle sizes and zeta potentials of the plain Sol NPs and Ag-AZI-Sol NPs (n = 3)

Condition	Plain Sol	Ag-AZI-Sol
Average diameter (nm)	54.3 ± 3.6	134.3 ± 5.6
Zeta potential (mV)	−18.9 ± 0.5	−13.1 ± 0.5

Table 2 Conductivities of LIG electrodes obtained by varying the power and speed of the CO_2 laser

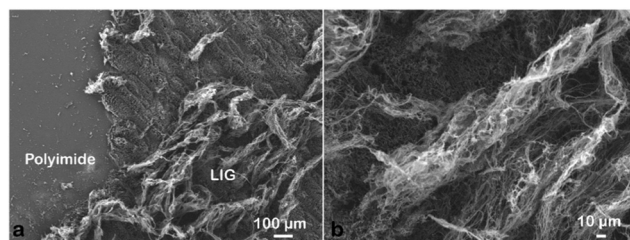| Power (%)	Speed (%)	Thickness (μm)	Resistivity (mΩ m)	Conductivity (S m^{-1})
10.0	10.0	117.8	7.9	125.1
	7.5	93.7	3.8	262.3
	5.0	75.8	1.8	543.4
	2.5	66.4	698.5	**1430.0**
7.5	10.0	99.8	8.4	117.6
	7.5	99.3	6.4	164.1
	5.0	106.1	3.3	297.1
	2.5	124.3	1.3	752.8
5.0	10.0	58.0	7.2	138.6
	7.5	60.0	4.2	234.2
	5.0	57.9	2.4	400.5
	2.5	76.0	1.4	712.4
2.5	10.0	—	—	—
	7.5	—	—	—
	5.0	—	—	—
	2.5	76.0	3.1	314.2

Fig. 3 SEM images of LIG obtained at a laser power of 10% (12 W) and a speed of 2.5% (0.105 m s^{-1}).
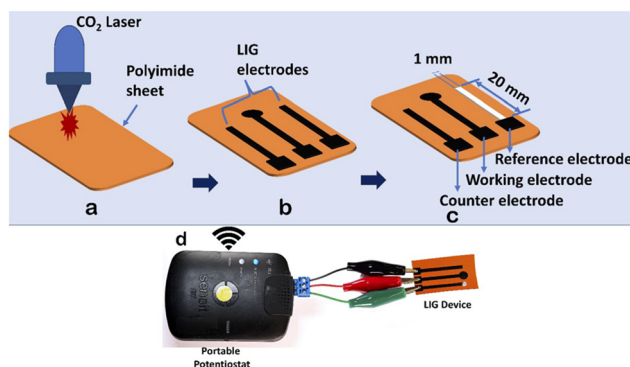

Fig. 4 (a) A bare polyimide sheet. (b) An Epilog laser used to engrave the polyimide sheet to form electrodes. (c) An electrode modified with Ag/AgCl ink acting as a reference electrode. (d) A snapshot of the setup.

of 100 μL was maintained throughout the electrochemical investigations.

3. Results and discussion

3.1 Morphological changes in bacteria induced by Ag-AZI-Sol NP treatment

The mechanism of Ag-AZI-Sol NPs penetrating the bacterial membrane is multifaceted.[31] Initially, Ag ions are released from the nanoparticles, interacting with the bacterial outer membrane and compromising its integrity through electrostatic interactions.[32] This disruption facilitates the penetration of Ag ions into the bacterial cell through passive diffusion or active transport mechanisms.[33,34] Once inside, the Ag ions target cellular components, leading to dysfunction and cell death. Additionally, the presence of azithromycin (AZI) may enhance the antimicrobial activity.[35]

This mechanism involves membrane disruption, intracellular penetration, and interference with cellular processes, ultimately inhibiting bacterial growth.[36] The impact of the released Ag ions on the bacterial outer membrane, disrupting its properties, is depicted in Fig. 5, illustrating microbial inhibition against both *S. epidermidis* (Gram-positive) and *E. coli* (Gram-negative).

Sol is an amphiphilic polymer known for its adhesive properties toward bacterial cells. When combined with Ag-AZI, it
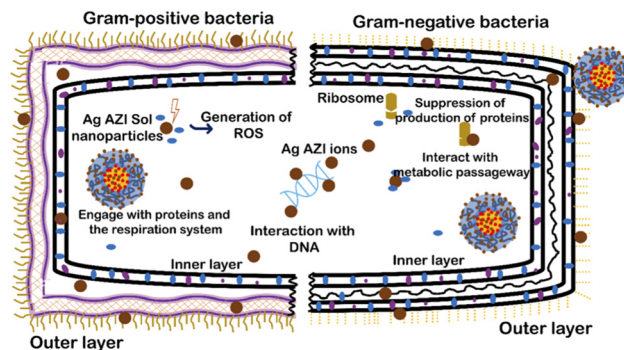

Fig. 5 Interaction of Ag-AZI-Sol NPs with Gram-positive and Gram-negative bacteria cell membranes.

enhances its collective ability to induce cellular damage. Previous studies have shown the surfactant effects of Sol NPs on bacterial cells.[37,38] The antibacterial activity of Ag-AZI-Sol operates through inhibition of bacterial protein synthesis by binding to the 50S ribosomal subunit. Additionally, the Ag-AZI-Sol NPs release silver ions, which are the primary contributors to bacterial inactivation. Initially, silver ions damage the bacterial cell membrane, followed by subsequent damage to DNA, proteins, and enzymes.

SEM analysis was employed to investigate morphological and structural alterations in the bacterial cells following treatment with Ag-AZI-Sol NPs. Prior to SEM analysis, the samples were treated with a hydrophilic ionic liquid, enhancing the conductivity and facilitating clear imaging of biological samples.[39] This method has been demonstrated to provide high-resolution images suitable for biological analysis. *E. coli* and *S. epidermidis* biofilms were grown in a 24-well plate. After forming the biofilms, Ag-AZI-Sol NP suspensions (5 and 10 mg mL^{-1}) in a medium were added to each well. After the nanoparticle treatment, the cells were incubated for 2 h and 6 h at 37 °C with 0.5% CO_2.

In our previous study,[24] *S. epidermidis* cells were found to display circular 3D structures with a diameter of 1 μm. The extracellular polymeric substance (EPS), composed of polysaccharides, plays a crucial role in biofilm formation. Following treatment with Ag-AZI-Sol NPs at a concentration of 5 μg mL^{-1} for 2 hours, as shown in Fig. 6a, the particles infiltrated the bacterial cells while the EPS film began to deteriorate. The Ag-Sol NPs adhered to the bacterial cell boundary, inducing alterations in cell morphology. After 6 hours of treatment, as depicted in Fig. 6b, the Ag-AZI-Sol NPs were clearly observed between the bacterial cells, causing significant changes in cell morphology. The cells became non-circular and flat with no discernible cell division, and the EPS structure completely faded.

Next, investigations were carried out using a higher concentration of 10 μg mL^{-1} of Ag-AZI-Sol NPs on *S. epidermidis* for 2 hours (Fig. 6c) and 6 hours (Fig. 6d). Comparable results were observed, although the bacterial cells tended to flatten at the higher concentration of 10 μg mL^{-1}.

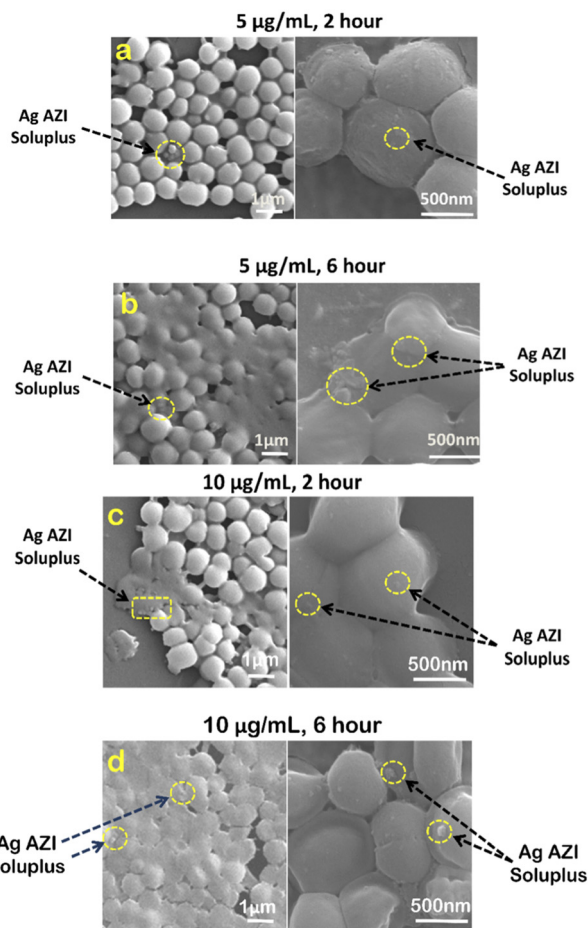**Fig. 6** SEM images of *S. epidermidis* with 5 μg mL^{-1} and 10 μg mL^{-1} of Ag-AZI-Sol NPs after (a, c) 2 hours and (b, d) 6 hours.

Examinations were also conducted on *E. coli* treated with 5 μg mL^{-1} of Ag-AZI-Sol NPs. Fig. 7a illustrates the cell structure after 2 hours of treatment, depicting the Ag-AZI-Sol NPs attached to the biofilms while the EPS film remains largely intact. However, after 6 hours of treatment, as shown in Fig. 7b, the *E. coli* bacterial cells were visibly damaged, with the Ag-AZI-Sol NPs adhering to them.
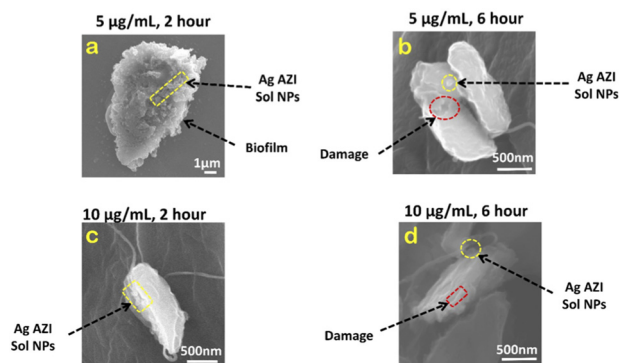

Fig. 7 SEM images of *E. coli* with 5 μg mL^{-1} and 10 μg mL^{-1} of Ag-AZI-Sol NPs after (a, c) 2 hours and (b, d) 6 hours.

Furthermore, the effects on *E. coli* were examined using a higher concentration of 10 μg mL^{-1} of Ag-AZI-Sol NPs for 2 hours (Fig. 7c) and 6 hours (Fig. 7d). Partially damaged bacterial cells were observed after 2 hours of treatment, with a noticeable flattening of the cells observed after 6 hours.

3.2 Antibacterial assay studies

Antibacterial assays were performed using a LIVE/DEAD BacLight bacterial viability kit. Biofilms of *E. coli* and *S. epidermidis* were grown in a 24-well plate using LB medium, washed with purified water, and then treated with Sol NPs, Ag-AZI-Sol NPs, Ag NPs, and Ag-Sol-NPs for 2 hours. To examine the effects of different dosing times, Ag-AZI-Sol NPs were also applied for 0, 30, 120, 240, and 360 minutes. The detailed procedure is described elsewhere.[40]

Fluorescence was measured using a multimode detector (DTX880, Beckman Coulter Co., USA). Three wells were measured per sample, and each measurement was repeated three times. The excitation/emission wavelengths were 488/535 nm (green) for SYTO 9 and 485/625 nm (red) for propidium iodide. The ratio of green to red fluorescence was compared with a standard viability cell line to determine the percentage of viable cells.

The equation obtained from the standard viability cell line was used to calculate the percentages of viable cells after various treatments ($n = 3$). Variance equality between the two populations was assessed using an F-test,[41] followed by a two-sample t-test with equal variances.[42] In the case of *E. coli*, the antibacterial effect was less pronounced compared to *S. epidermidis* (Fig. 8a–d). At a dose of 5 μg mL^{-1} of Ag-AZI-Sol NPs for 2 hours, more than 60% of live bacterial cells remained viable (Fig. 8a and b). The SEM results revealed a persistent thick EPS film after this treatment duration. However, a greater antibacterial effect was observed with longer treatment durations and higher concentrations of Ag-AZI-Sol NPs (Fig. 8c and d).

The antibacterial assay results demonstrated the potent antibacterial activity of Ag-AZI-Sol NPs against *S. epidermidis* biofilms (Fig. 9a–d). After 2 hours of treatment with 5 μg mL^{-1} of Ag-AZI-Sol NPs, only a small percentage of live bacterial cells remained viable, as depicted in Fig. 9a and b. SEM analysis corroborated these findings, showing the reduction of EPS and flattening of bacterial cells in the bacterial morphology.

3.3 Microorganism growth analysis using optical measurements

We examined the impact of Ag-AZI-Sol NPs on bacterial viability by treating *E. coli* (Gram-negative) and *S. epidermidis* (Gram-positive) with concentrations of 5 and 10 μg mL^{-1}. Upon treatment, the Ag-AZI-Sol NPs promptly released Ag ions, increasing the release rate over time (refer to section 2.4). As depicted in Fig. 10b and 11b, the Ag-AZI-Sol NPs exhibited dose-dependent antibacterial activity against *E. coli* and *S. epidermidis*. In Fig. 10b, the growth of *E. coli* growth with and without (control) the Ag-AZI-Sol NPs is illustrated. The OD
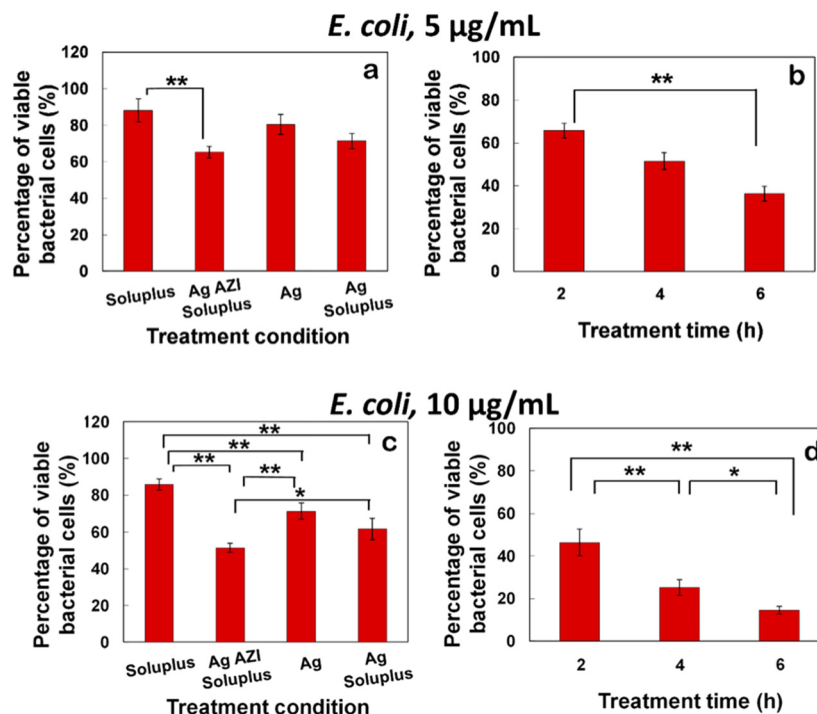
Fig. 8 Percentages of viable *E. coli* bacterial cells after various treatments (Sol NPs, Ag-AZI-Sol NPs, Ag NPs and Ag-Sol NPs). Ag concentration: (a) 5 μg mL^{-1} and (c) 10 μg mL^{-1} for 2 h. Percentage of viable bacterial cells after Ag-AZI-Sol NP treatment. Ag concentration: (b) 5 μg mL^{-1} and (d) 10 μg mL^{-1} for 2 h, 4 h and 6 h, respectively. Data are shown as the mean ± SD (n = 3). ** Significant difference between each treatment ($p < 0.01$).
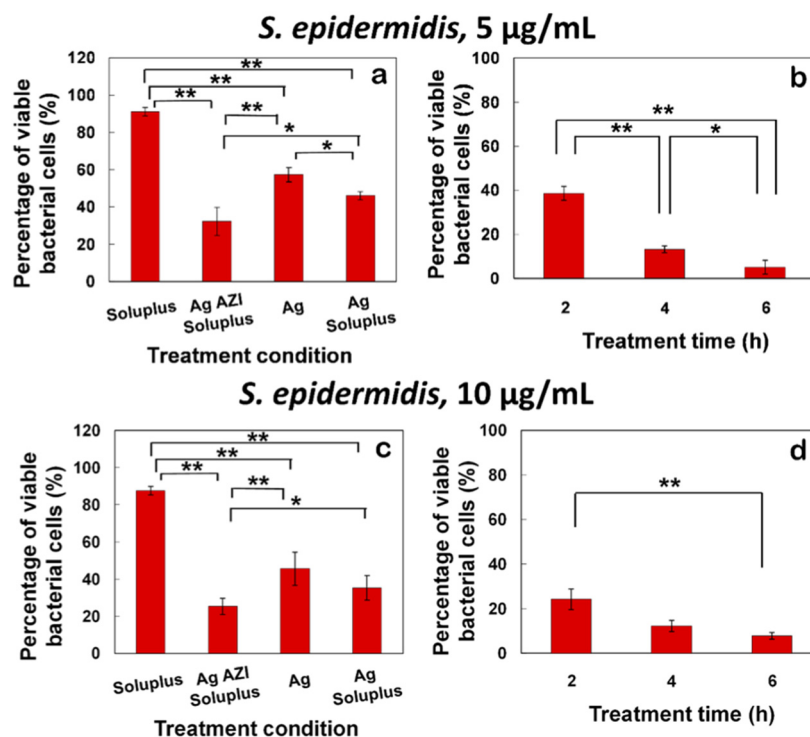

Fig. 9 Percentages of viable *S. epidermidis* bacterial cells after various treatments (Sol NPs, Ag-AZI-Sol NPs, Ag NPs and Ag-Sol NPs). Ag concentration: (a) 5 μg mL^{-1} and (c) 10 μg mL^{-1} for 2 h. Percentage of viable bacterial cells after Ag-AZI-Sol NP treatment. Ag concentration: (b) 5 μg mL^{-1} and (d) 10 μg mL^{-1} for 2 h, 4 h and 6 h, respectively. Data are shown as the mean ± SD (n = 3). ** Significant difference between each treatment ($p < 0.01$).
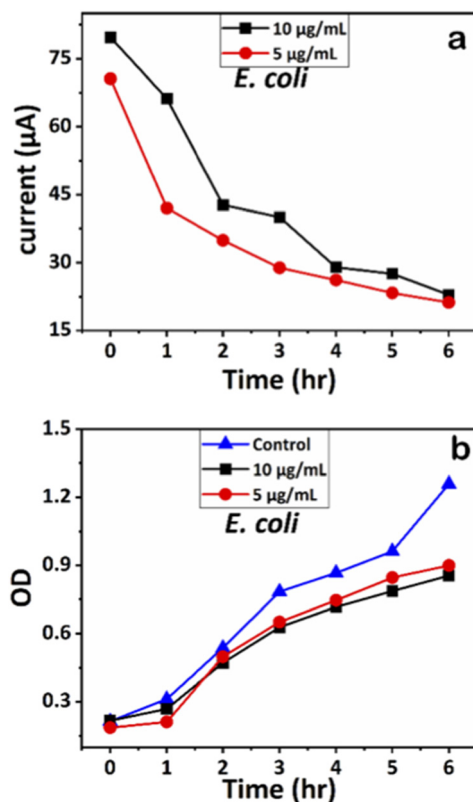
Fig. 10 (a) Chronoamperometry readings of *E. coli* and (b) growth analysis of *E. coli* with the control using OD measurements.
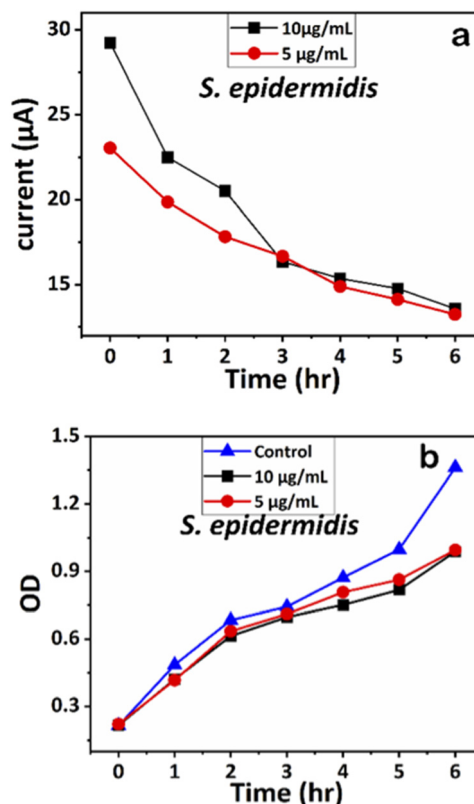

Fig. 11 (a) Chronoamperometry readings of *S. epidermidis* and (b) growth analysis of *S. epidermidis* with the control using OD measurements.

values for the control were higher than the OD value obtained at Ag AZI Sol NPs at concentration of 10 μg mL^{-1}.

Similarly, the influence of Ag-AZI-Sol NPs on *S. epidermidis* was assessed using OD measurements (Fig. 11b). Both concentrations (5 and 10 μg mL^{-1}) exhibited comparable antibacterial effects up to the sixth hour. These results validated further the effect of Ag-AZI-Sol NPs over microbial growth.[43]

3.4 LIG-based electrochemical analysis of antibacterial properties using Ag-AZI-Sol NPs

Since the discovery of laser-induced graphene (LIG), researchers have been exploring its diverse applications,[44,45] particularly in antibacterial research.

Singh *et al.* conducted experimental analysis, revealing that LIG, composed of carbon nanofibers sized between 250 and 750 nm with micropores ranging from 1 to 25 μm, exhibited remarkable antibacterial properties, particularly against bacterial proliferation. Comparative studies between crushed and non-crushed LIG surfaces highlighted the latter's efficacy in inhibiting biofilm formation, suggesting that LIG's microporous structure plays a crucial role in biofilm resistance and bacteria capture.[46] Another study demonstrated enhanced antibacterial activity of LIG when doped with Ag.[47,48] Huang *et al.* developed a face mask using LIG, demonstrating its superior antibacterial capacity against *E. coli* and *S. epidermidis*.[27] Further investigations involved modifying LIG with zinc oxide (ZnO) and Ag-doped ZnO

nanocrystals, revealing significant antibacterial effectiveness against pathogens such as *E. coli* and *S. aureus*.[28,49]

Leveraging these properties, we developed a miniaturized electrochemical platform employing CO$_2$ laser technology to explore antibacterial activity through chronoamperometry measurements. This platform, integrated with a portable potentiostat, as shown in Fig. 4d, facilitated the real-time monitoring of bacterial activity. The chronoamperometry technique was used to analyze bacterial activity for 6 hours with the following optimized parameters: applied potential (E_{dc}) = 0.95 V and run time (t_{run}) = 180 seconds. For the electrochemical experiments, two concentrations of Ag-AZI-Sol NPs, 5 μg mL^{-1} and 10 μg mL^{-1}, were selected, along with *E. coli* and *S. epidermidis* cultures at an optical density of 0.2 OD. The synthesized Ag-AZI-Sol NPs were dispersed in the freshly prepared LB media. Equal volumes of the Ag-AZI-Sol NP solution and bacterial culture were mixed and sonicated for 1 minute. A 100 μL sample of the mixture was subjected to chronoamperometry testing every hour for up to six hours. The chronoamperometry parameters, including the equilibrium time ($t_{equilibrium}$ = 0 s, E_{dc} = 0.95 V, $t_{interval}$ = 0.1s) and the run time (t_{run} = 180s), were optimized for these experiments. The initial chronoamperometry reading for both *E. coli* and *S. epidermidis* was measured at 180 s. Subsequently, a mixture of bacteria and particles was returned to the incubator to allow bacterial growth in the presence of Ag-AZI-Sol particles.

The corresponding current readings from the chronoamperometry were recorded hourly until the sixth hour, with the stable currents for *E. coli* shown in Fig. 10a and those for *S. epidermidis* shown in Fig. 11a. We observed a declining trend in current values across all concentrations of Ag-AZI-Sol NPs in the presence of bacteria.

The highly conductive nature of our LIG electrodes, which exhibit a conductivity of 1430 S m^{-1}, enhances our ability to detect subtle changes in current when in contact with bacteria. The porous structure of the LIG, coupled with its large surface area, provides numerous active microsites for interfacing with bacteria such as *E. coli* and *S. epidermidis*. Electrostatic interactions between the LIG and the bacterial cell membranes influence the observed current values: more active bacterial contact correlates with higher currents, while less active contact results in lower currents. In the initial two hours, as detailed in section 3.1, the Ag ions predominantly target the bacterial cell membranes, leading to a notable decrease in current. Subsequently, the Ag ions penetrate the cellular interior, disrupting proteins, respiratory functions, and DNA, which is reflected in the gradual decline in current. This trend indicates that higher concentrations of Ag-AZI-Sol NPs were more effective in bacterial inactivation compared to lower concentrations.

4. Conclusions

The solvent emulsion diffusion method employed in this study successfully produced Ag-AZI-Sol NPs, characterized by a size range of 200 nm and the sustained release of Ag ions for up to six hours. These released Ag ions exhibited potential antibacterial activity against *E. coli* and *S. epidermidis*. SEM analysis provided initial evidence of the high antibacterial efficacy of Ag-AZI-Sol NPs, revealing clear morphological changes in microorganisms at concentrations of 5 and 10 μg mL^{-1}. Moreover, as corroborated by SEM analysis, the Ag-AZI-Sol NPs demonstrated an ability to penetrate the outer cell membrane of microorganisms and remain within the bacterial cell. Further confirmation was obtained through anti-bacterial assay, spectrophotometry and electrochemical analyses which effectively validated the antibacterial efficacy of Ag-AZI-Sol NPs against Gram-negative and Gram-positive bacteria. This study supports the potential application of Ag-AZI-Sol NPs in various industries, including food processing and medical device manufacture, offering promising avenues for combating bacterial contamination and enhancing product safety.

Author contributions

M. M. J.: conceptualization, experiments, data analysis, and writing; C. T.: conceptualization, experiments, data curation, data analysis, resources, and writing; B. H.: methodology (exp.), review, and edit; A. Q. S.: conceptualization (exp.), resources, writing, review, and editing.

Data availability

The data that support the findings of this study are available from the corresponding authors, Dr Chisato Takahashi and Dr Amy Q. Shen, upon reasonable request. Additionally, any supplementary information required to reproduce the results reported in this study can also be obtained from the corresponding author.

Conflicts of interest

The authors declare there is no conflict of interest.

Acknowledgements

References

1 L. K. Vestby, T. Grønseth, R. Simm and L. L. Nesse, *Antibiotics*, 2020, **9**, 59.

2 P. J. Weldick, A. Wang, A. F. Halbus and V. N. Paunov, *Nanoscale*, 2022, **14**, 4018–4041.

3 K. K. Jefferson, *FEMS Microbiol. Lett.*, 2004, **236**, 163–173.

4 S. A. Brennan, C. Ní Fhoghlú, B. M. Devitt, F. J. O'Mahony, D. Brabazon and A. Walsh, *Bone Joint J.*, 2015, **97-B**, 582–589.

5 D. Roe, B. Karandikar, N. Bonn-Savage, B. Gibbins and J.-B. Roullet, *J. Antimicrob. Chemother.*, 2008, **61**, 869–876.

6 Z. Khatoon, C. D. McTiernan, E. J. Suuronen, T.-F. Mah, E. I. Alarcon and E. I. Alarcon Bacterial, *Heliyon*, 2018, **4**, e01067.

7 S. P. Usha, H. Manoharan, R. Deshmukh, R. Álvarez-Diduk, E. Calucho, V. V. R. Sai and A. Merkoçi, *Chem. Soc. Rev.*, 2021, **50**, 13012–13089.

8 K. Markowska, A. M. Grudniak and K. I. Wolska, *Acta Biochim. Pol.*, 2013, **60**, 523–530.

9 R. Javed, M. Zia, S. Naz, S. O. Aisida, N. ul Ain and Q. Ao, *J. Nanobiotechnol.*, 2020, **18**, 1–15.

10 S. Iravani, H. Korbekandi, S. V. Mirmohammadi and B. Zolfaghari, *Res. Pharm. Sci.*, 2014, **9**(6), 385–406.

11 L. Wang, M. Hasanzadeh Kafshgari and M. Meunier, *Adv. Funct. Mater.*, 2020, **30**(51), 2005400.

12 F. Beck, M. Loessl and A. J. Baeumner, *Microchim. Acta*, 2023, **190**, 91.

13 K. Plaeyao, R. Kampangta, Y. Korkokklang, C. Talodthaisong, A. Saenchoopa, S. Thammawithan,

K. Latpala, R. Patramanon, N. Kayunkid and S. Kulchat, *RSC Adv.*, 2023, **13**, 19789–19802.

14   D. Astruc, *Chem. Rev.*, 2020, **120**, 461–463.

15   R. R. Miranda, I. Sampaio and V. Zucolotto, *Colloids Surf., B*, 2022, **210**, 112254.

16   A. Wasilewska, M. Bielicka, U. Klekotka and B. Kalska-Szostko, *Food Funct.*, 2023, **14**, 2544–2567.

17   A. Istiqola and A. Syafiuddin, *J. Chin. Chem. Soc.*, 2020, **67**, 1942–1956.

18   E. Valentin, A. L. Bottomley, G. S. Chilambi, E. J. Harry, R. Amal, G. A. Sotiriou, S. A. Rice and C. Gunawan, *Nanoscale*, 2020, **12**, 2384–2392.

19   S. H. Lee and B. H. Jun, *Int. J. Mol. Sci.*, 2019, **20**(4), 865.

20   P. Bélteky, A. Rónavári, N. Igaz, B. Szerencsés, I. Y. Tóth, I. Pfeiffer, M. Kiricsi and Z. Kónya, *Int. J. Nanomed.*, 2019, **14**, 667–687.

21   M. Rehan, H. M. Mashaly, M. S. Abdel-Aziz, R. M. Abdelhameed and A. S. Montaser, *Cellulose*, 2024, 1–32.

22   H. Kang, J. T. Buchman, R. S. Rodriguez, H. L. Ring, J. He, K. C. Bantz and C. L. Haynes, *Chem. Rev.*, 2019, **119**, 664–699.

23   C. Takahashi, T. Yamada, S. Yagi, T. Murai and S. Muto, *Mater. Sci. Eng., C*, 2021, **121**, 111718.

24   C. Takahashi, S. Saito, A. Suda, N. Ogawa, Y. Kawashima and H. Yamamoto, *RSC Adv.*, 2015, **5**, 71709–71717.

25   Z. Zhang, H. Zhu, W. Zhang, Z. Zhang, J. Lu, K. Xu, Y. Liu and V. Saetang, *Carbon*, 2023, **214**, 118356.

26   S. Beikzadeh, A. Akbarinejad, J. Taylor, S. Swift, D. Simonov, J. Ross, J. Perera, P. A. Kilmartin and J. Travas-Sejdic, *Appl. Mater. Today*, 2023, **31**, 101753.

27   L. Huang, S. Xu, Z. Wang, K. Xue, J. Su, Y. Song, C. Zhu, Z. Tang and R. Ye, *ACS Nano*, 2020, **14**, 12045–12053.

28   J. Lin, Z. Peng, Y. Liu, F. Ruiz-Zepeda, R. Ye, E. L. G. Samuel, M. J. Yacaman, B. I. Yakobson and J. M. Tour, *Nat. Commun.*, 2014, **5**, 5714.

29   R. Ye, D. K. James and J. M. Tour, *Acc. Chem. Res.*, 2018, **51**, 1609–1620.

30   Y. Chyan, R. Ye, Y. Li, S. P. Singh, C. J. Arnusch and J. M. Tour, *ACS Nano*, 2018, **12**, 2176–2183.

31   M. A. Radzig, V. A. Nadtochenko, O. A. Koksharova, J. Kiwi, V. A. Lipasova and I. A. Khmel, *Colloids Surf., B*, 2013, **102**, 300–306.

32   K. Mijnendonckx, N. Leys, J. Mahillon, S. Silver and R. Van Houdt, *BioMetals*, 2013, **26**, 609–621.

33   A. Salleh, R. Naomi, N. D. Utami, A. W. Mohammad, E. Mahmoudi, N. Mustafa and M. B. Fauzi, *Nanomaterials*, 2020, **10**, 1–20.

34   P. R. More, S. Pandit, A. De Filippis, G. Franci, I. Mijakovic and M. Galdiero, *Microorganisms*, 2023, **11**(2), 369.

35   Y. Zhang, X. Pan, S. Liao, C. Jiang, L. Wang, Y. Tang, G. Wu, G. Dai and L. Chen, *J. Proteome Res.*, 2020, **19**, 3109–3122.

36   V. Pareek, R. Gupta and J. Panwar, *Mater. Sci. Eng., C*, 2018, **90**, 739–749.

37   D. J. Hess, M. J. Henry-Stanley and C. L. Wells, *Antimicrob. Agents Chemother.*, 2014, **58**, 6970–6973.

38   I. M. Banat, M. A. D. De Rienzo and G. A. Quinn, *Appl. Microbiol. Biotechnol.*, 2014, **98**, 9915–9929.

39   C. Takahashi, G. Kalita, N. Ogawa, K. Moriguchi, M. Tanemura, Y. Kawashima and H. Yamamoto, *Anal. Bioanal. Chem.*, 2014, **407**, 1607–1613.

40   C. Takahashi, N. Ogawa, Y. Kawashima and H. Yamamoto, *Microscopy*, 2015, **64**, 169–180.

41   A. De Beuckelaer, *A closer examination on some parametric alternatives to the ANOVA F-test*, Springer-Verlag, 1996, vol. 37.

42   P. Mishra, U. Singh, C. M. Pandey, P. Mishra and G. Pandey, *Ann. Card. Anaesth.*, 2019, **22**, 407–411.

43   L. Yang, W. Yan, H. Wang, H. Zhuang and J. Zhang, *RSC Adv.*, 2017, **7**, 11355–11361.

44   N. H. Barbhuiya, A. Kumar and S. P. Singh, *Trans. Indian Natl. Acad. Eng.*, 2021, **6**, 159–171.

45   V. P. Wanjari, A. S. Reddy, S. P. Duttagupta and S. P. Singh, *Environ. Sci. Pollut. Res.*, 2023, **30**, 42643–42657.

46   S. P. Singh, S. Ramanan, Y. Kaufman and C. J. Arnusch, *ACS Appl. Nano Mater.*, 2018, **1**, 1713–1720.

47   A. Gupta, L. Holoidovsky, C. Thamaraiselvan, A. K. Thakur, S. P. Singh, M. M. Meijler and C. J. Arnusch, *Chem. Commun.*, 2019, **55**, 6890–6893.

48   S. Beikzadeh, A. Akbarinejad, J. Taylor, S. Swift, D. Simonov, J. Ross, J. Perera, P. A. Kilmartin and J. Travas-Sejdic, *Appl. Mater. Today*, 2023, **31**, 101753.

49   D. Wang, J. Li, Y. Wang, F. Liu, G. Wang, X. Ding, S. Luo and G. Chen, *ACS Appl. Nano Mater.*, 2022, **5**, 6841–6851.